Received 5 February 2006
Revised 2 January 2007
Accepted 2 January 2007

Population balance models for subcooled boiling flows

M.K.M. Ho and G.H. Yeoh
Australian Nuclear Science and Technology Organisation (ANSTO), Menai, Australia, and
J.Y. Tu
School of Aerospace, Mechanical and Manufacturing Engineering, RMIT University, Bundoora, Australia

Abstract

Purpose – This study aims to examine both the population balance approach based on the MUltiple SIze Group (MUSIG) model and the average bubble number density transport equation (ABND) model for 3D, low pressure, gas-liquid, subcooled boiling, vertical flows. The purpose is to assess the ability of both models to predict the radial profile of void fraction, bubble Sauter mean diameter and interfacial area concentration which characterise subcooled boiling.

Design/methodology/approach – Improvement in the ABND model to simulate gas-liquid bubbly flows with heat transfer was achieved by combining the condensation expression with the gaseous mass transport equation within the CFD commercial code CFX4.4.

Findings – Overall, both the ABND model and the MUSIG model provided good results in terms of the above-mentioned criteria when compared against experimental measurements. However, the ABND model was found to have limitations in predicting high-subcooled boiling flows due to the lack of bubble size resolution to adequately capture the effect of condensation over a range of bubbles sizes.

Originality/value – It is shown that the ABND model provides an economic alternative to the MUSIG model in terms of complexity and computational time, as long as one is aware of the limitations in simulating high-subcooling flow regimes.

Keywords Modelling, Boiling, Flow, Thermodynamics

Paper type Research paper

Nomenclature

A_C = cross sectional area of boiling channel
a_{if} = interfacial area concentration
D_s = bubble Sauter mean diameter
f = bubble departure frequency
f_i = scalar variable of the dispersed phase
g = gravitational acceleration
h = inter-phase heat transfer coefficient
G = mass flux
N'' = active nucleation site density
h_{fg} = latent heat
H = enthalpy
k = turbulent kinetic energy
n_i = number density of the ith class
n_j = number density of the jth class
P = pressure
Q_w = wall heat flux
Q_c = heat transferred by convection
Q_e = heat transferred by evaporation
Q_q = heat transferred by quenching
S_i = source term due to coalescence and break-up
T = temperature
T_{sat} = saturation temperature
T_{sub} = subcooling temperature
u = velocity
$\vec{\mathbf{u}}$ = velocity vector
v = volume corresponding to particle diameter d

Greek symbols

α = void fraction
ε = dissipation of kinetic energy

International Journal of Numerical Methods for Heat & Fluid Flow
Vol. 18 No. 2, 2008
pp. 160-172

0961-5539
DOI 10.1108/09615530810846310

Γ = mass transfer
λ = size of an eddy
μ = dynamic viscosity
μ^e = effective viscosity
ρ = density
$\Delta\rho$ = density difference $(\rho_l - \rho_g)$
ξ_H = heated parameter

Subscripts
g = vapour
gl = transfer of quantities from liquid phase to vapour phase
l = liquid
lg = transfer of quantities from vapour phase to liquid phase
min = minimum

Introduction

Crucial to the safe operation of the high-flux Australian research (HIFAR) reactor and open pool Australian light water research (OPAL) reactor at Australian Nuclear Science and Technology Organisation (ANSTO) is the ability to accurately model thermohydraulic accident scenarios. Thermohydraulic safety analyses of HIFAR and OPAL requires the examination of subcooled boiling flow regimes in the reactor core. Subcooled boiling occurs when the bulk liquid temperature remains below the liquid saturation temperature, with nucleation occurring at the wall of the reactor fuel elements. Traditionally, one-dimensional reactor thermohydraulic safety codes utilised flow mapping to characterise reactor flow behaviour. This capability has been increased recently with the release of a 3D thermohydraulic code utilising the MUltiple SIze Group (MUSIG) model. This is beneficial as it allows the examination of radial profiles of void fraction and bubble Sauter mean diameter, as opposed to obtaining only averaged axial results. An alternative to the MUSIG model is the one group average number density equation model. This code has, however, yet to be thoroughly validated when coupled with subcooled boiling mechanisms.

To model subcooled boiling, wall nucleation mechanisms accounting for bubble growth and condensation mechanisms accounting for bubble volume decay due to subcooling are incorporated into the MUSIG and the ABND model in CFX4.4. Three different theoretical expressions for bubble coalescence and break-up by Wu *et al.* (1998), Hibiki *et al.* (2001) and Yao and Morel (2004) were incorporated into the ABND model and compared against the MUSIG model by Yeoh and Tu (2005) and experimental results by Lee *et al.* (2002). It has often been debated as to which population balance model should be used in the CFD modelling of gas-liquid bubbly flows (Lo, 1996). Proponents for the MUSIG model argue for the need for bubble size resolution. Whilst some industrial practitioners of CFD find the average number density equation model quite adequate. This study seeks to compare the two models and highlight the relative qualities of both.

Theory

The numerical representation of the two-fluid model for bubbly flows can be thought of as two fluids superimposed on one another to form one continuum. The two fluids are each represented by a set of conservation equations for mass, momentum and energy. These equations are similarly represented in the MUSIG model and the ABND model.

- *continuity equation of liquid phase (common):*

$$\frac{\partial \rho_l \alpha_l}{\partial t} + \nabla \cdot (\rho_l \alpha_l \vec{\mathbf{u}}_l) = \Gamma_{lg} \tag{1}$$

- *continuity equation of vapour phase ABND model:*

$$\frac{\partial \rho_g \alpha_g}{\partial t} + \nabla \cdot (\rho_g \alpha_g \vec{\mathbf{u}}_g) = S_i - \Gamma_{lg} \quad \text{single averaged bubble size} \tag{2}$$

- *continuity equation of vapour phase MUSIG model:*

$$\frac{\partial \rho_g \alpha_g f_i}{\partial t} + \nabla \cdot (\rho_g \alpha_g \vec{\mathbf{u}}_g f_i) = S_i - f_i \Gamma_{lg} \quad \text{multiple bubble sizes} \tag{3}$$

- *momentum equation of liquid phase (common):*

$$\begin{aligned} \frac{\partial \rho_l \alpha_l \vec{\mathbf{u}}_l}{\partial t} + \nabla \cdot (\rho_l \alpha_l \vec{\mathbf{u}}_l \vec{\mathbf{u}}_l) = & - \alpha_l \nabla P + \alpha_l \rho_l \vec{g} + \nabla \cdot \left[\alpha_l \mu_l^e (\nabla \vec{\mathbf{u}}_l + (\nabla \vec{\mathbf{u}}_l)^T) \right] \\ & + (\Gamma_{lg} \vec{\mathbf{u}}_g - \Gamma_{gl} \vec{\mathbf{u}}_l) + F_{lg} \end{aligned} \tag{4}$$

- *momentum equation of vapour phase (common):*

$$\begin{aligned} \frac{\partial \rho_g \alpha_g \vec{\mathbf{u}}_g}{\partial t} + \nabla \cdot (\rho_g \alpha_g \vec{\mathbf{u}}_g \vec{\mathbf{u}}_g) = & - \alpha_g \nabla P + \alpha_g \rho_g \vec{g} + \nabla \cdot \left[\alpha_g \mu_g^e (\nabla \vec{\mathbf{u}}_g + (\nabla \vec{\mathbf{u}}_g)^T) \right] \\ & + (\Gamma_{gl} \vec{\mathbf{u}}_l - \Gamma_{lg} \vec{\mathbf{u}}_g) + F_{gl} \end{aligned} \tag{5}$$

- *energy equation of liquid phase (common):*

$$\frac{\partial \rho_l \alpha_l H_l}{\partial t} + \nabla \cdot (\rho_l \alpha_l \vec{\mathbf{u}}_l H_l) = \nabla \cdot \left[\alpha_l \lambda_l^e \nabla T_l \right] + (\Gamma_{lg} H_g - \Gamma_{gl} H_l) \tag{6}$$

- *energy equation of vapour phase (common):*

$$\frac{\partial \rho_g \alpha_g H_g}{\partial t} + \nabla \cdot (\rho_g \alpha_g \vec{\mathbf{u}}_g H_g) = \nabla \cdot \left[\alpha_g \lambda_g^e \nabla T_g \right] + (\Gamma_{gl} H_l - \Gamma_{lg} H_g) \tag{7}$$

Since, mass, momentum and energy are transferred between the bulk liquid and bubbles during nucleation and condensation, interphase transfer terms are necessary to maintain closure within the conservation expressions. The interphase transfer term Γ_{lg} in equation (1) allows for the transfer of mass due to condensation and is proportional to the interphase heat transfer coefficient h, the interfacial area concentration (IAC) a_{if}, the amount of subcooling ($T_{sat} - T_l$) and is inversely proportional to the latent heat transfer coefficient h_{fg}. It is expressed as:

$$\Gamma_{lg} = \frac{h a_{if} (T_{sat} - T_l)}{h_{fg}} \tag{8}$$

The mass transfer due to nucleation Γ_{gl} accounts for all vapour bubbles generated at the heated wall and is modelled by considering the heat transfer due to evaporation Q_e, the latent heat transfer coefficient h_{fg}, the liquid specific heat C_{pl} and the subcooled temperature $T_{sub} = (T_{sat} - T_l)$. It is expressed as:

$$\Gamma_{gl} = \frac{Q_e}{h_{fg} + C_{pl} T_{sub}} \tag{9}$$

The interphase mass transfer term for nucleation Γ_{gl} does not appear in equations (2) or (3) but is accounted as a specified boundary condition apportioned to the discrete bubble class based on the size of the bubble departure criteria on the heated surface.

On the RHS of equations (2) and (3), S_i denotes the additional source terms due to coalescence and breakage of bubbles. Here, the coalescence rate of Prince and Blanch (1990) and break-up rate of Luo and Svendsen (1996) are, respectively, applied. For the former, bubble merging proceeds due to turbulent collision in the inertial sub-range of isotropic turbulence while for the latter, the so-called daughter bubble size fragmentation caused by the interaction of the bubbles with turbulent eddies is considered. Detailed expressions of these rates can be found in Yeoh and Tu (2005). The term $f_i\Gamma_{lg}$ represents the mass transfer due to condensation and is redistributed for each of the discrete bubble classes. The gas void fraction and scalar fraction f_i are related to the number density of the discrete bubble ith class n_i (similarly to the jth class n_j) as $\alpha_g f_i = n_i v_i$. The size distribution of the dispersed phase is thus defined by the scalar f_i. The inter-phase transfer terms in the momentum and energy equations Γ_{lg} and F_{lg} denote the transfer terms from the gas phase to the liquid phase. The mass transfer Γ_{lg} is as explained in equation (7) whilst the total interfacial force F_{lg} considered in the present study includes the effects of:

$$F_{lg} = F_{lg}^{drag} + F_{lg}^{lift} + F_{lg}^{lubrication} + F_{lg}^{dispersion} \tag{10}$$

The total interfacial force F_{lg} is composed of the drag force, lift force, wall lubrication force and the turbulent dispersion force, respectively. A detailed description of these forces is provided by Anglart and Nylund (1996) and Lahey and Drew (2001).

The k-ε turbulence model is used for the liquid and dispersed vapour continuum. The effective viscosity in the momentum and energy equations is taken as the sum of the molecular viscosity and turbulent viscosity. The turbulent viscosity is considered as the total of the shear-induced turbulent viscosity and Sato *et al.*'s (1981) bubble-induced turbulent viscosity.

The wall heat flux Q_w is composed of three components: the heat transferred by conduction to the superheated layer next to the wall, Q_q; the heat transferred by evaporation or vapour generation, Q_e; and the heat transferred by turbulent convection, Q_c. Details of the wall heat flux is provided by Yeoh and Tu (2005). The local bubble Sauter mean diameter based on the calculated values of the scalar fraction f_i and discrete bubble sizes d_i is calculated by:

$$D_s = \frac{1}{\sum_i f_i / d_i} \tag{11}$$

The ABND bubble coalescence and break up mechanisms

In this study, three different bubble coalescence and break up mechanisms, as formulated by Wu *et al.* (1998), Hibiki *et al.* (2001) and Yao and Morel (2004), are compared with the results of subcooled boiling MUSIG model.

Wu *et al.* modelled bubble coalescence due to the effect of both random collisions driven by turbulence (RC) and wake entrainment (WE), as expressed by:

$$\phi_n^{\mathrm{CO}} = \phi_n^{\mathrm{RC}} + \phi_n^{\mathrm{WE}}.$$

While the mechanisms responsible for bubble breakage is caused by the impact of turbulent eddies (TI), as shown by:

$$\phi_n^{\mathrm{BK}} = \phi_n^{\mathrm{TI}}.$$

These three mechanisms of coalescence and breakage developed by Wu *et al.* have the form:

$$\phi_n^{\mathrm{RC}} = -0.021 \frac{\alpha_{\mathrm{g}}^2 \varepsilon^{1/3}}{D_{\mathrm{s}}^{11/3} \alpha_{\max}^{1/3} \left(\alpha_{\max}^{1/3} - \alpha_{\mathrm{g}}^{1/3}\right)} \left[1 - \exp\left(-\frac{\alpha_{\max}^{1/3} \alpha_{\mathrm{g}}^{1/3}}{\alpha_{\max}^{1/3} - \alpha_{\mathrm{g}}^{1/3}}\right)\right] \tag{12}$$

$$\phi_n^{\mathrm{WE}} = -0.0073 U_r \frac{\alpha_{\mathrm{g}}^2}{D_{\mathrm{s}}^4} \tag{13}$$

$$\phi_n^{\mathrm{TI}} = 0.0945 \frac{\alpha_{\mathrm{g}} \varepsilon^{1/3}}{D_{\mathrm{s}}^{11/3}} \exp\left(1 - \frac{We_{\mathrm{cr}}}{We}\right) \exp\left(\frac{We_{\mathrm{cr}}}{We}\right) \tag{14}$$

where $\alpha_{\max}$ is the maximum allowable void fraction of 0.80, U_{r} is the relative velocity between the gas and liquid phases, We is the Weber number and We_{cr} is the critical Weber number of 2.0.

Based on experimental observations, Hibiki *et al.* (2001) and Yao and Morel (2004) did not consider wake entrainment as a part of their bubble coalescence mechanism, as coalescence due to wake entrainment was observed to be significant only between pairs of large capped bubbles in slug flow. Hibiki and Ishii's coalescence and break up mechanisms thus have the form:

$$\phi_n^{\mathrm{CO}} = -0.03 \frac{\alpha_{\mathrm{g}}^2 \varepsilon^{1/3}}{D_{\mathrm{s}}^{11/3} (\alpha_{\max} - \alpha_{\mathrm{g}})} \exp\left(-1.29 \frac{\rho_{\mathrm{l}}^{1/2} \varepsilon^{1/3} D_{\mathrm{s}}^{5/6}}{\sigma^{1/2}}\right) \tag{15}$$

$$\phi_n^{\mathrm{BK}} = 0.03 \frac{\alpha_{\mathrm{g}} (1 - \alpha_{\mathrm{g}}) \varepsilon^{1/3}}{D_{\mathrm{s}}^{11/3} (\alpha_{\max} - \alpha_{\mathrm{g}})} \exp\left(-1.37 \frac{\sigma}{\rho_l \varepsilon^{2/3} D_{\mathrm{s}}^{5/3}}\right) \tag{16}$$

whereas Yao and Morel's coalescence and break up mechanisms were derived to be:

$$\phi_n^{\mathrm{CO}} = -2.86 \frac{\alpha_{\mathrm{g}}^2 \varepsilon^{1/3}}{D_{\mathrm{s}}^{11/3}} \frac{\exp\left(-1.017 \sqrt{We/We_{\mathrm{cr}}}\right)}{\left(\alpha_{\max}^{1/3} - \alpha_{\mathrm{g}}^{1/3}\right) \Big/ \alpha_{\max}^{1/3} + 1.922 \alpha_{\mathrm{g}} \sqrt{We/We_{\mathrm{cr}}}} \tag{17}$$

$$\phi_n^{\mathrm{BK}} = 1.6\frac{\alpha_g(1-\alpha_g)\varepsilon^{1/3}}{D_s^{11/3}}\ \frac{\exp(-(We)/(We_{cr}))}{1+0.42(1-\alpha_g)\sqrt{We/We_{cr}}} \tag{18}$$

The maximum allowable void fraction of both Hibiki and Ishii and Yao and Morel's models is 0.52, which is the void fraction at the transitional region between spherical bubble flow and capped bubble flow. The critical Weber number in Yao and Morel's model in equation (18) is set to a value of 1.24.

The population balance model

The population balance equation for the MUSIG model has been described by Yeoh and Tu (2005). Here, the ABND form of the population balance model can be derived as:

$$\frac{\partial \rho_g \alpha_g n}{\partial t} + \nabla \cdot (\rho_g \alpha_g \vec{\mathbf{u}}_g n) = \Gamma_{lg}.n + \phi^{\mathrm{CO}} + \phi^{\mathrm{BK}} \tag{19}$$

where n is the bubble number density, ϕ^{co} and ϕ^{BK} are the bubble coalescence and breakage terms and Γ_{lg} is the mass transfer due to condensation. At the heated wall, bubbles are formed at the activated cavities known as activated nucleation sites. The spawning of bubbles at the heated wall proportionally increases the bubble number density in control volumes adjacent to the heated wall. Thus, an increase in bubble number density, as calculated by equation (20) is fed into the bubble number density n in equation (19) for control volumes adjacent to the heated wall. The nucleation rate is evaluated as a specified boundary condition as shown below in equation (20):

$$\phi_{\mathrm{WN}} = \frac{N'' f \xi_H}{A_C} \tag{20}$$

where N'' is the active nucleation site density, f is the bubble generation frequency from active sites, ξ_H is the heated parameter, and A_C is the cross-sectional area of the boiling channel. A detailed description can be obtained from the previous work by Yeoh and Tu (2005).

Experimental and numerical details

The numerical model was validated against experiments conducted by Lee *et al.* (2002). As shown in Figure 1, the test section of the experimental rig consisted of a vertical cylinder 37.5 mm in diameter and 2,376 mm high. Located concentrically is an inconel 625 tube, 19 mm in diameter, which is heated by a 54 kW DC power supply. Demineralised water was used as the working fluid. The measuring plane is located at 1.61 m downstream of the beginning of the heated section and a 50 mm transparent section of the outer cylinder is located just before the measuring plane to allow for visual observations. Uncertainties of void fraction and liquid and gas velocity measurements were approximated to be at 3 per cent but bubble Sauter mean diameter measurement uncertainty was estimated to be a little less than 27 per cent. Experimental conditions that have been used for comparison with the simulated results are presented in Table I.

Solution to the two sets of governing equations for the balance of mass, momentum and energy of each phase was sought. Additional equations for the population balance

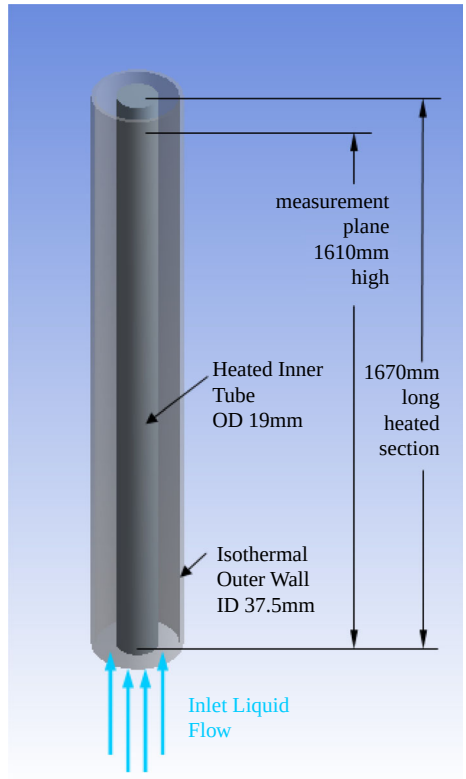

Figure 1.
Diagram of experiment conducted by Lee *et al.* (2002)

Case 1	P_{inlet} (MPa)	T_{inlet} (°C)	T_{sub} (inlet) (°C)	Q_w (kW/m^2)	G (kg/m^2 s)
C1	0.142	96.6	13.4	152.3	474.0
C2	0.137	94.9	13.8	197.2	714.4
C3	0.143	92.1	17.9	251.5	1,059.2

Table I.
Experimental conditions

approach were also solved. The conservation equations were discretised using the control volume technique. The velocity-pressure linkage was handled through the SIMPLE procedure. The discretised equations were solved using Stone's strongly implicit procedure (Sato *et al.*, 1981). Since, the wall heat flux was applied uniformly throughout the inner wall of the annular and taking advantage of the annular geometrical shape, only a quarter of the annular was considered as the domain for simulation. A body-fitted conformal system was employed to generate the three-dimensional mesh within the annular channel resulting in a total of 13 (radial) $\times$ 30 (height) $\times$ 3 (circumference) control volumes – effectively a 2D axisymmetric model. Grid independence was examined. For the mean parameters considered, further grid refinement did not reveal significant changes to the two-phase flow parameters.

Results and discussion

The measured and predicted radial profiles of the vapour void fraction, bubble Sauter diameter (D_s) and IAC are shown in Figures 2-5. Common to all figures is the radial position axis, with $(r - R_i)/(R_o - R_i) = 0$ representing the position of the inner heated wall and $(r - R_i)/(R_o - R_i) = 1$ representing the position of the outer unheated wall.

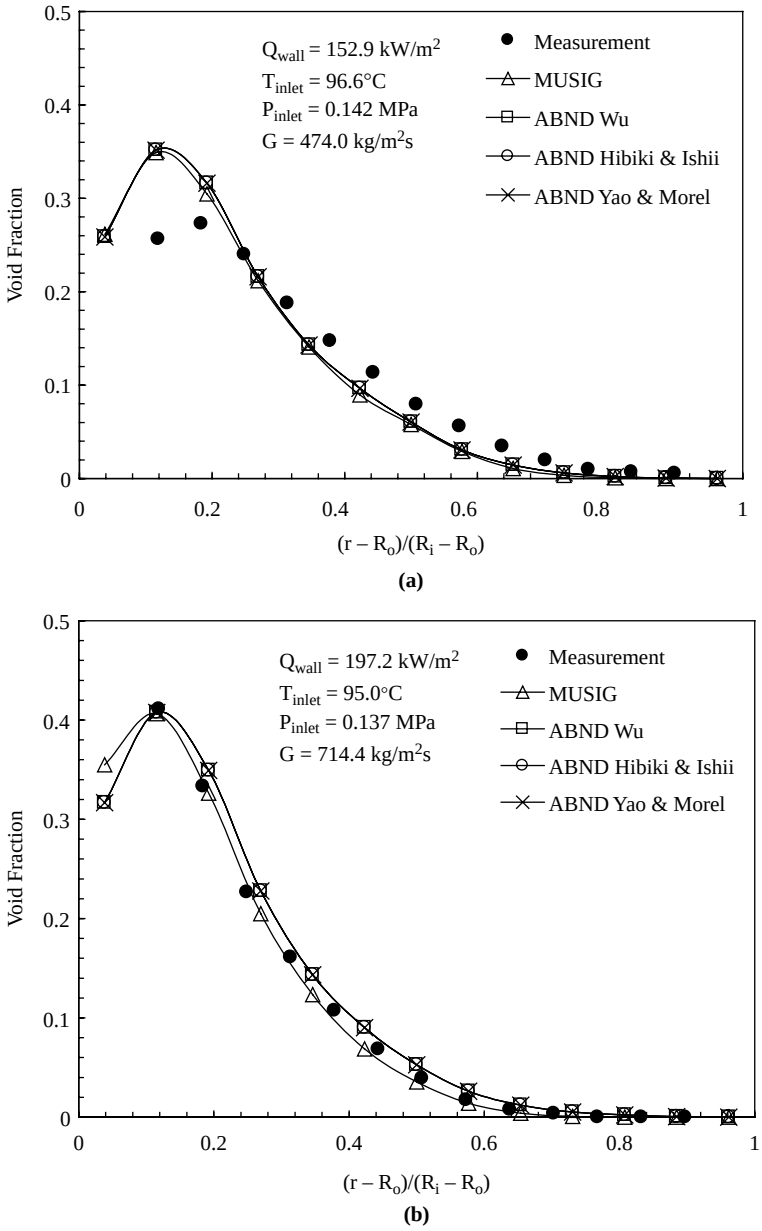

Figure 2.
Radial void fraction measurements for case 1 (a) and case 2 (b)

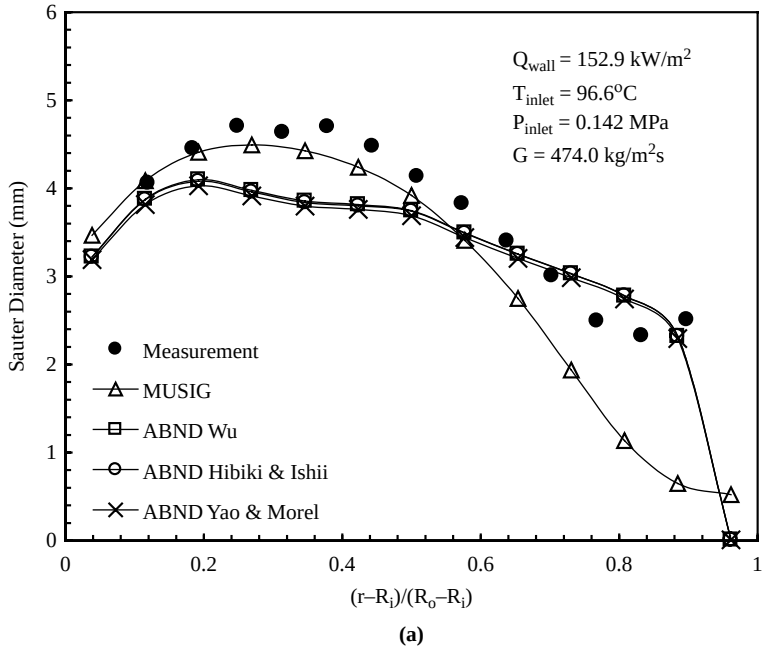

(a)

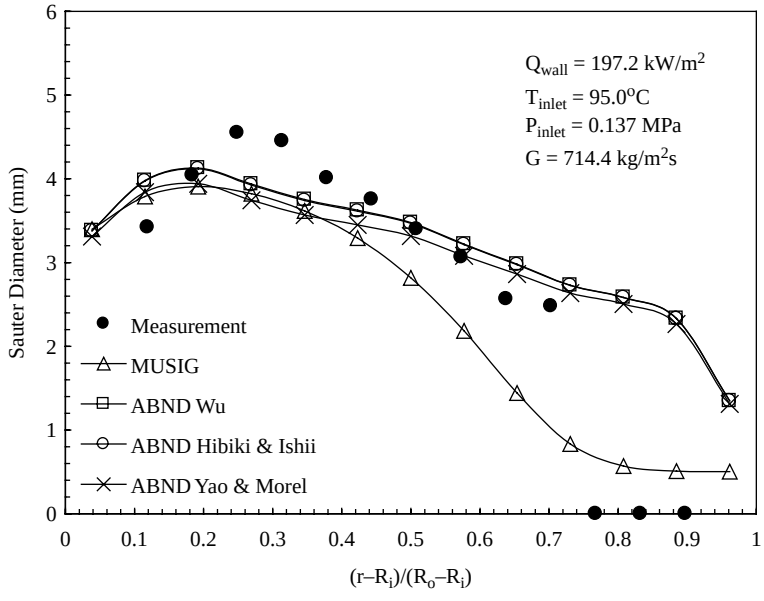

(b)

Figure 3.
Radial average bubble Sauter diameter for case 1 (a) and case 2 (b)

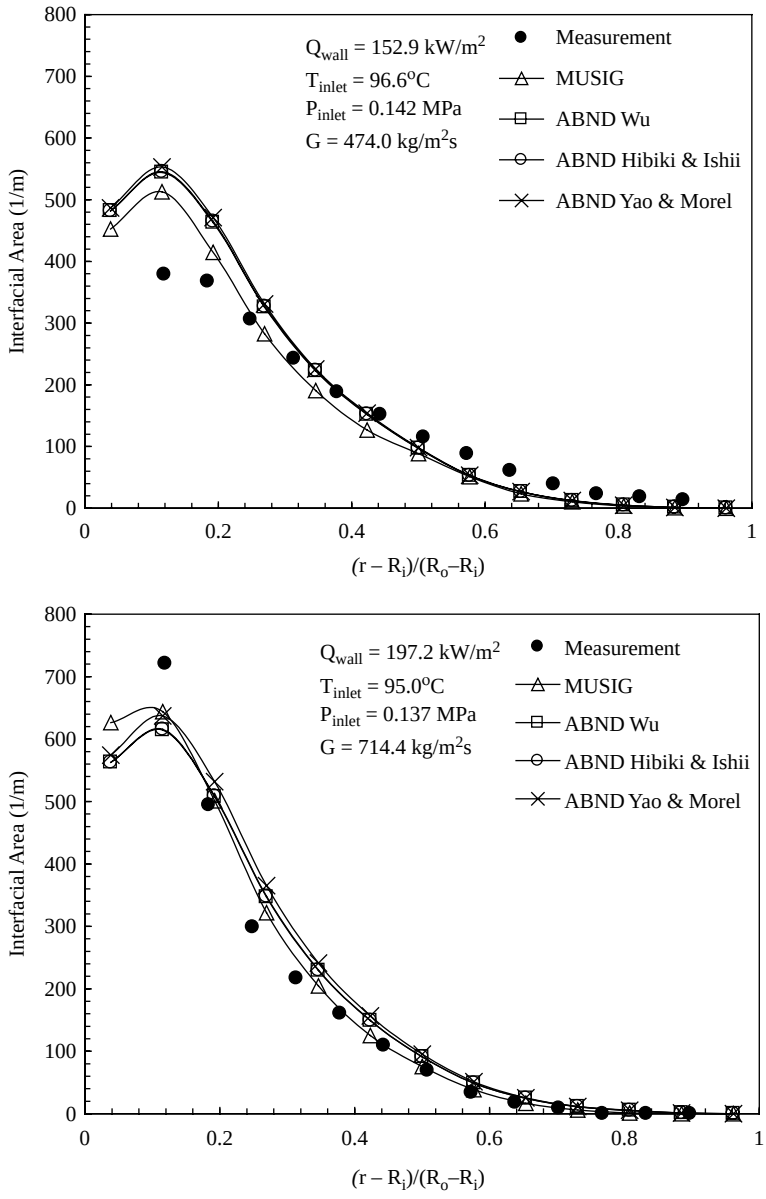

Figure 4.
Radial Interfacial area at exit for case 1 (a) and case 2 (b)

Both measured and predicted void fraction profiles of cases 1 and 2 (Figure 2) display typical subcooled boiling radial profiles, with an incidence of wall peaking near the heated wall due to nucleation and a decrease in void fraction away from the heated wall due to the action of condensation on bubbles in the subcooled liquid. It is suspected

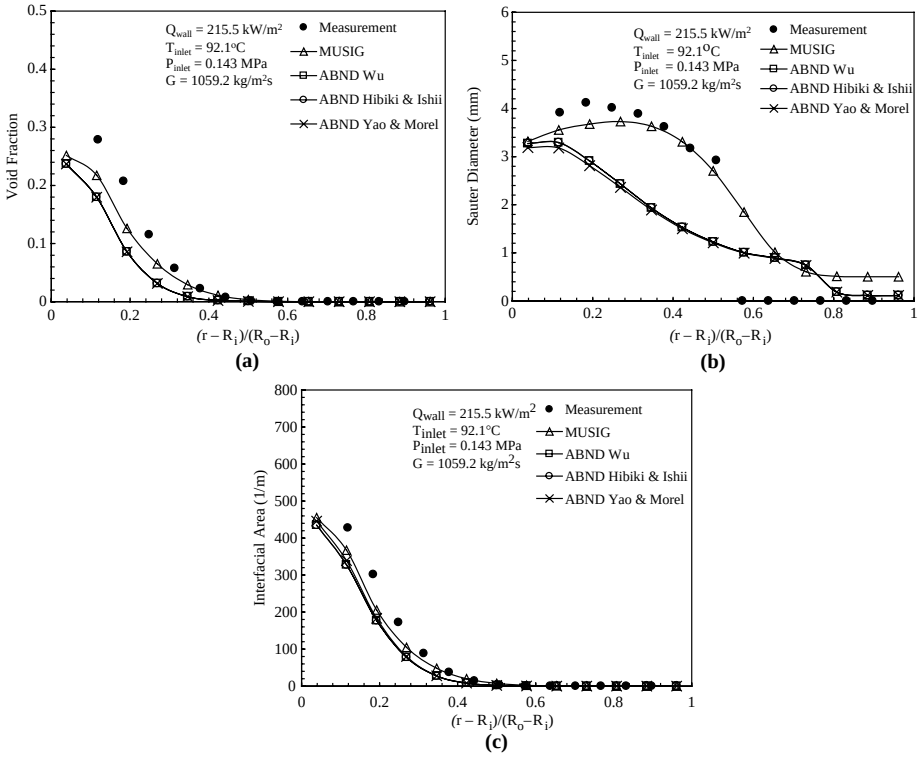

Figure 5.
(a) Case 3 void fraction; (b) case 3 bubble Sauter diameter; (c) case 3 IAC

that, the slightly higher wall peaking void fraction in case 1, Figure 2, is due to the limitations of a correlation-based expression for nucleation as shown by equation (20).

In Figure 3, for both cases 1 and 2, the ABND models gives slightly lower bubble Sauter mean diameter predictions when compared to measurements by Lee *et al.* However, this lower bubble Sauter diameter does not have such a detrimental effect on the IAC as shown in Figure 4 because the low-void fraction away from the heated wall is used to calculate the IAC in the expression $a_{if} = 6\alpha_g/D_s$. More importantly, given that the interphase mass transfer terms in the flow of equations (2) and (3) is reliant on the IAC a_{if} to calculate the change of water vapour to liquid as expressed by equation (8), it is the IAC prediction that is of influence when simulating the evolution of subcooled boiling flow regimes.

In case 3, the subcooling is higher than in cases 1 and 2 and this has had a perceivable effect on the bubble Sauter diameter predictions in the ABND models. As before, the bubble Sauter diameter is lower for the ABND models but due to high subcooling, the ABND average bubble size prediction for case 3 (Figure 5(b)) is markedly lower than in cases 1 and 2 (Figure 4). The lower than expected bubble size of the ABND model can be attributed to the limitation of bubble size resolution inherent to the ABND model. An average bubble size of the ABND model was unable to capture the varying rates of condensation for bubbles of different sizes.

This resulted in an under-predicted bubble diameter profile curve in Figure 5(b). The smaller ABND bubble size is also reflected in the slightly under-predicted ABND void fraction profile in Figure 5(a). As a result, this has caused the ABND IAC in Figure 5(c) to be slightly under-predicted as well.

Conclusion

Improvement in the ABND model to simulate gas-liquid bubbly flows with heat transfer has been made by combining the condensation expression with the gaseous mass transport equation within the CFD commercial code CFX4.4. Three forms of the ABND model incorporating theoretical expressions for bubble coalescence and breakage by Wu *et al.* (1998), Hibiki *et al.* (2001) and Yao and Morel (2004) were compared against the MUSIG model by Yeoh and Tu (2005) and experimental results by Lee *et al.* (2002). It was found that for low subcooling all three ABND models gave results comparable with the MUSIG model. However, in higher subcooling regimes, it was discovered that the single average bubble size of an ABND model could not capture the high-condensation effect on a range of bubble sizes. This resulted in an under-predicted bubble Sauter diameter profile, which is also reflected in slightly under-predicted void fraction and IAC profiles. Benefits with using the ABND model can be gained for its relative simplicity in implementation and savings in computational time. Thus, in so far one is aware of the limitation of ABND model in predicting high-subcooled boiling flows, the ABND model can be found as capable as the MUSIG model for simulating subcooled boiling flows.

References

Anglart, H. and Nylund, O. (1996), "CFD application to prediction of void distribution in two-phase bubbly flows in rod bundles", *Nuc. Sci. Eng.*, Vol. 163, pp. 81-98.

Hibiki, T., Ishii, M. and Xiao, Z. (2001), "Axial interfacial area transport of vertical bubbly flow", *Int. J. Heat Mass Transfer*, Vol. 41, pp. 1869-88.

Lahey, R.T. Jr and Drew, D.A. (2001), "The analysis of two-phase flow and heat transfer using multidimensional, four field, two-fluid model", *Nuc. Eng. Design*, Vol. 204, pp. 29-44.

Lee, T.H., Park, G.-C. and Lee, D.J. (2002), "Local flow characteristics of subcooled boiling flow of water in a vertical annulus", *Int. J. Multiphase Flow*, Vol. 28, pp. 1351-68.

Lo, S. (1996), "Application of population balance to CFD modelling of bubbly flow via the MUSIG model", AEAT-1096, AEA Technology, Abingdon.

Luo, H. and Svendsen, H. (1996), "Theoretical model for drop and bubble break-up in turbulent dispersions", *AIChE J.*, Vol. 42, pp. 1225-33.

Prince, M.J. and Blanch, H.W. (1990), "Bubble 'coalescence and break-up in air-sparged bubble column'", *AIChE J.*, Vol. 36, pp. 1485-99.

Sato, Y., Sadatomi, M. and Sekoguchi, K. (1981), "Momentum and heat transfer in two-phase bubbly flow – I", *Int. J. Multiphase Flow*, Vol. 7, pp. 167-78.

Wu, Q., Kim, S., Ishii, M. and Beus, S.G. (1998), "One-group interfacial area transport in vertical bubbly flow", *Int. J. Heat Mass Transfer*, Vol. 41, pp. 1103-12.

Yao, W. and Morel, C. (2004), "Volumetric interfacial area prediction in upwards bubbly two-phase flow", *Int. J. Heat Mass Transfer*, Vol. 47, pp. 307-28.

Yeoh, G.H. and Tu, J.Y. (2005), "Thermal-hydraulic modelling of bubbly flows with heat and mass transfer", *AIChE J.*, Vol. 51, pp. 8-27.

Further reading

Tomiyama, A. (1998), "Struggle with 'computational bubble dynamics'", paper presented at ICMF'98, 3rd Int. Conf. Multiphase Flow, Lyon, pp. 1-18.

About the authors

M.K.M. Ho graduated from the University of Technology, Sydney and holds and Master of Engineering by research (UTS) in reactor flow induced vibrations. He is working full time at ANSTO as a Thermo-hydraulic Analyst for the OPAL research reactor and supporting facilities. Currently, he is in the course of finishing his PhD studies part-time in the study of heat and mass transfer of bubbly flows with interface tracking at the University of New South Wales, Australia. M.K.M. Ho is the corresponding author and can be contacted at: Mark.Ho@ansto.gov.au

G.H. Yeoh graduated with a BEng degree (First Class Honours) in Mechanical Engineering from University of New South Wales (UNSW), Australia, and obtained his PhD from the same university later on. He has over 15 years of research experience in industry, has given many prominent seminar presentations at academic institutions/organisations world wide, and is currently a Senior Research Scientist at ANSTO. His areas of expertise are: computational fluid dynamics (CFD), nuclear reactor safety, fire engineering, mechanical ventilation and multiphase flows. He has received a prestigious award from NASA and is currently writing three books. Over 100 international refereed publications in areas of his expertise have been published.

J.Y. Tu graduated with a BEng (Hons) and MEngSci degree in Mechanical Engineering from Northeast University, China, and a PhD from The Royal Institute of Technology, Sweden. He has over 20 years of teaching and research experience in industry and at universities world wide, and is currently the Chair of School Postgraduate Research in School of Aerospace, Mechanical and Manufacturing Engineering at RMIT University, Australia. He has extensive research experience in the area of CFD and its application to a broad aspect of engineering including automotive, nuclear, defence and biomedical engineering. He is a recipient of several prestigious fellowship awards by Australian Academy of Science, Japan Society for the Promotion of Science, and Korea Science and Engineering Foundation. He has over 130 international refereed publications in areas of his expertise.